Synthesis and gas sensing properties of ZnO single crystal flakes

Ying Liu,[a] Jian Dong,[a] Peter J. Hesketh[b] and Meilin Liu*[a]

We report a new two-dimensional structure, ZnO single crystal flakes, synthesized using a simple combustion CVD process. The flakes grew upward from the Si substrate. The as-grown ZnO flakes were less than 200 nm thick and 10–20 μm wide. Unlike most 1-D ZnO structures with [0001] growth direction, ZnO flakes grow along $<10\bar{1}0>$ directions. A gas sensor based on a 200 nm thick ZnO flake exhibited fast response–recovery and high sensitivity to ethanol vapor. These as-synthesized single crystal ZnO flakes could have important technological applications.

Introduction

Because of its unique properties (*e.g.*, wide direct bandgap of E_g = 3.2 eV, piezoelectric and semiconducting behavior), ZnO has found numerous applications, including UV light-emitters, solar cells, transparent high power electronics, piezoelectric transducers, and gas sensors. As one of the earliest discovered and well-established gas sensing oxides,[1] ZnO has been extensively studied for the detection of inflammable or toxic gases such as H_2, C_2H_5OH, CO and NO_x.[2–5] It has been recognized that gas sensors based on nanostructured fibrous ZnO exhibited greater sensitivities and faster response than those based on their bulk counterparts.[6–8] Similarly, a single ZnO nanowire photodetector showed several orders of magnitude increase in conductance upon exposure to UV light. Development in integrated and smart systems requires a direct integration of sensor elements or sensor arrays with signal processing unit within a single chip to achieve higher sensitivity and selectivity. Thus miniaturization of active sensing elements is essential.[9] To date, bulk single crystals, 1-D nanostructures, and 0-D nanoparticles of ZnO have been synthesized and tested for various applications. It is believed that the high surface to volume ratio renders these structures spectacular properties. In this paper, we report a new 2-D ZnO structure, single crystal ZnO flakes of 50 nm to 1 μm thick, synthesized using a combustion chemical vapor deposition (CVD) process. Further, a tiny gas sensor has been fabricated by placing a fraction of a ZnO flake on interdigitated electrodes on a silicon substrate. The sensor demonstrated high signal to noise ratio and fast response–recovery to ethanol vapor.

ZnO has a hexagonal (wurtzite) crystal structure with a = 3.25 Å and c = 5.12 Å. Each Zn atom is tetrahedrally coordinated to four O atoms. Zn and O atoms alternately occupy crystallographic planes, forming layered structure. Therefore, anisotropic growth is expected in several crystallographic directions, including $<2\bar{1}\bar{1}0>$, $<10\bar{1}0>$, and $<0001>$. One-dimensional ZnO nanostructures such as nanowires, nanobelts, and nanorings have been reported in literature.[10–13] Hexagonal ZnO single crystals with {0001} exposure surfaces and $<2\bar{1}\bar{1}0>$, $<10\bar{1}0>$ growth directions, are energetically favored. Large, 2-D structures could form in this way.

Experimental

ZnO single crystal flakes were synthesized using a combustion vapor condensation process as described elsewhere.[14–17] The experimental apparatus for combustion CVD is schematically illustrated in Fig. 1. Zinc nitrate (from Aldrich) is dissolved in ethanol with a concentration of 0.005 M. The solution is then delivered to an atomizer where a fine mist of solution is generated and combusted with the assistance of a small methane flame. Si slices (1 cm × 1 cm) cut from a Si wafer were used as substrates. A type K thermocouple is placed in the vicinity of the substrate surface to monitor deposition temperature. Depositions were performed at 1100 °C for 30 min. The as-grown ZnO flakes were characterized using a scanning electron microscope (SEM, LEO 1530 Thermally-Assisted FEG) with an energy dispersive spectroscopy (EDS) attachment, a transmission electron microscope (TEM, JEOL 100C), and an X-ray diffractometer (XRD, Phillips PW-1800).

The as-synthesized ZnO flakes were scratched into an ethanol bath, ultrasonically dispersed and broken into smaller pieces. A drop of the suspension was transported to patterned Pt electrodes and dried naturally. The dropping process was repeated until a single ZnO flake could be observed bridging
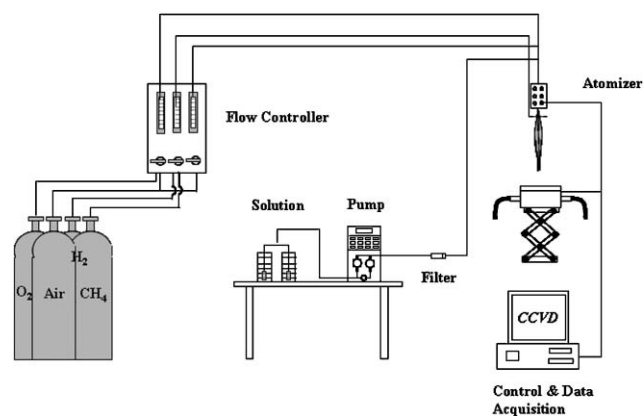

Fig. 1 A schematic of combustion CVD process.

*meilin.liu@mse.gatech.edu

two electrodes. The sensor was tested in ethanol vapor (300 and 500 ppm balanced by air) at 400 °C at a gas flow rate of 100 sccm. The current flowing through the ZnO flake was measured using a Solartron 1255 Electrochemical Interface at an applied constant voltage of 100 mV.

Results and discussion

Shown in Fig. 2 are some typical morphologies of the as-synthesized ZnO flakes. These ZnO flakes were randomly and fairly uniformly distributed on the substrate (Fig. 2a). An angular view (Fig. 2b) more clearly shows that ZnO flakes are oriented upward with respect to the underlying substrate. The higher magnification image (Fig. 2c) shows that each ZnO flake has a cactus-like shape with the maximum dimension of

15 to 20 μm on the top and gradually narrowing down to the bottom. Fig. 2d shows a SEM micrograph of a single ZnO flake. The thickness of the ZnO flakes can be up to 1 μm as shown in Fig. 2d or as thin as 150 to 250 nm (Fig. 2e, 2f). The large surface appears to be very smooth while the peripheral surfaces are faceted, showing a hexagonal pattern. These features indicate each ZnO flake probably is a single crystal with {0001} flat surface.

The composition of the as-synthesized product was analyzed by SEM/EDX. As shown in Fig. 3a, only Zn was detected. Typical XRD pattern shown in Fig. 3b indicates that the product has wurtzite structure with cell constants of $a = 3.25$ Å and $c = 5.20$ Å (JCPDS card 03-0888).

These characteristics were further confirmed by TEM analysis. Shown in Fig. 4a is a TEM bright field image
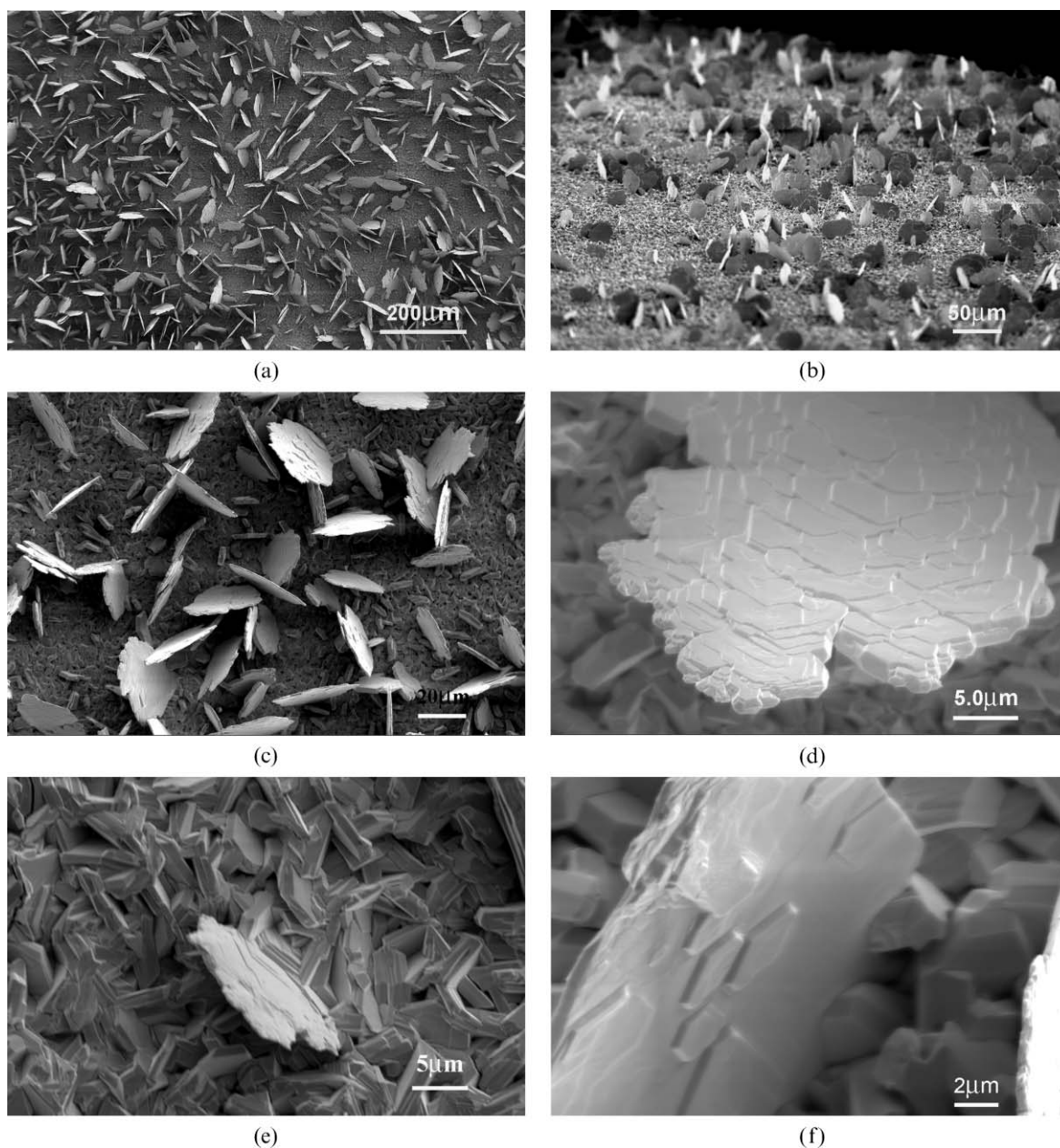
Fig. 2 SEM images of ZnO flakes synthesized at 1100 °C using a combustion CVD process.
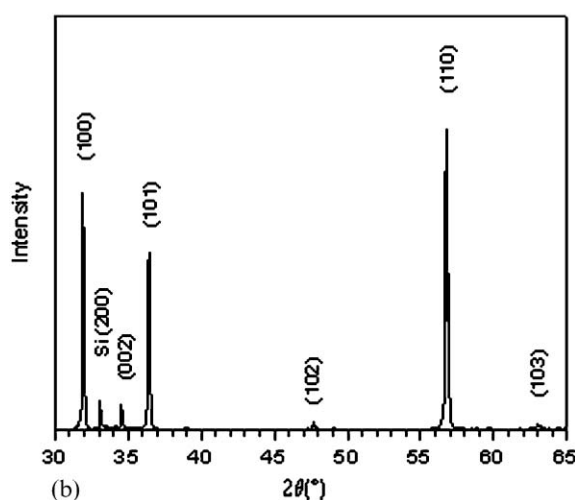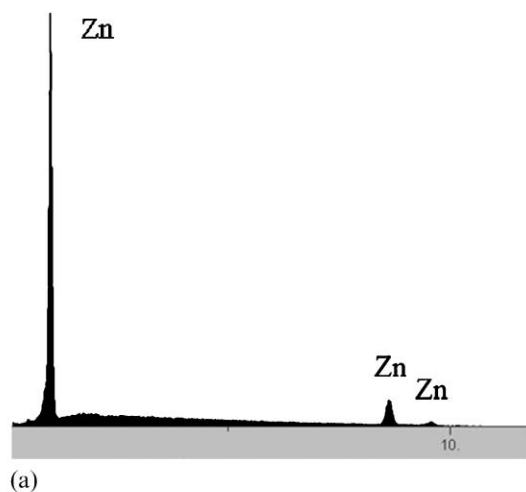
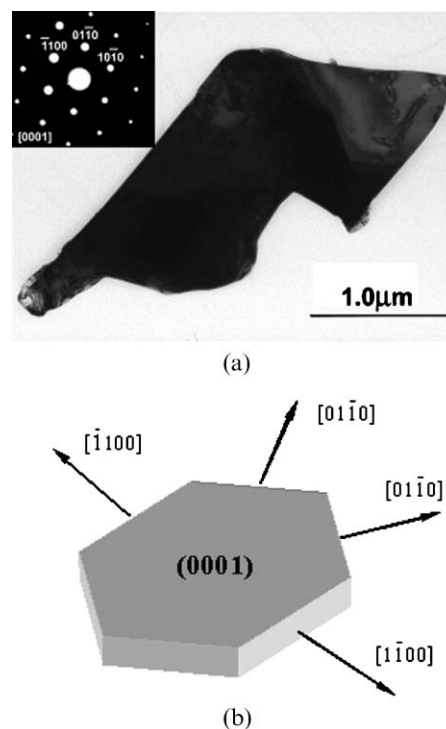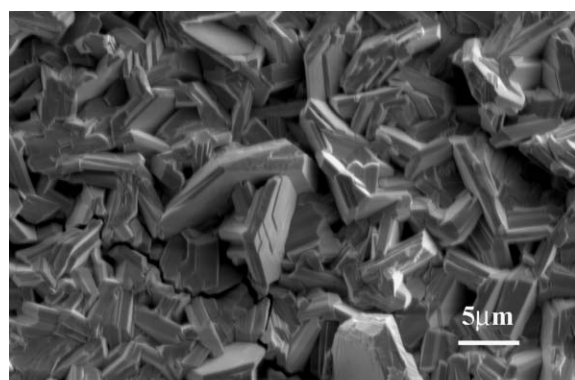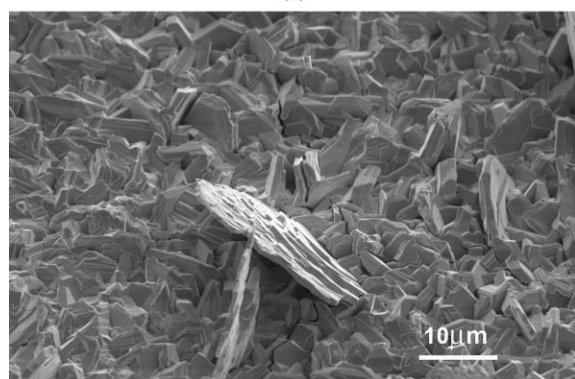Fig. 3 (a) EDX analysis of the ZnO flakes, and (b) XRD spectra.

Fig. 4 (a) TEM image and the corresponding SAED pattern of a ZnO single crystal flake, and (b) a schematic showing the preferential growth orientation of ZnO flakes.
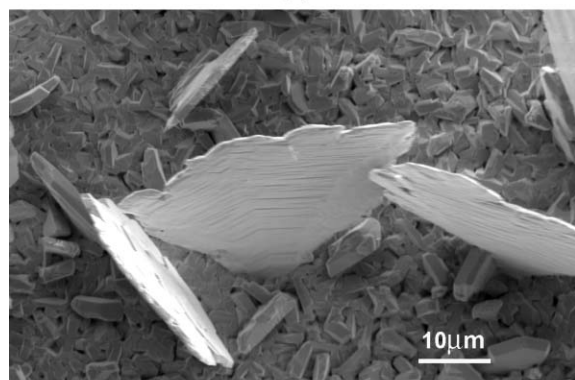
together with an inset showing the corresponding selected area electron diffraction (SAED) pattern, indicating that each ZnO flake is a single crystal with wurtzite structure. The peripheral facets intersecting one another at approximately 120 °C were identified as $\{10\bar{1}0\}$ planes. The corresponding zone axis was determined to be [0001].

As a wurtzite structure, ZnO typically has three fast growth directions, $<2\bar{1}\bar{1}0>$, $<10\bar{1}0>$, and $<0001>$, corresponding to three low energy crystallographic planes, $\{2\bar{1}\bar{1}0\}$, $\{10\bar{1}0\}$, and $\{0001\}$ respectively. Preferential growth in a particular direction is under kinetic control of synthesis conditions. For ZnO wire or rod-like structures, the growth predominantly follows $<0001>$ orientation, independent of pre-introduced catalysts.[10,11,18–20] In this case, lateral surface planes are sets of $\{2\bar{1}\bar{1}0\}$ or $\{10\bar{1}0\}$ planes, resulting in a hexagonal appearance. The growth direction of $<2\bar{1}\bar{1}0>$ was observed in ZnO nanobelts where $\{0001\}$ planes form the two larger peripheral surfaces.[21] The other two $\{10\bar{1}0\}$ peripheral surfaces did not grow significantly. In our situation, except the dominating lateral $\{0001\}$ surfaces, all the fast growth fronts were covered by $\{10\bar{1}0\}$ facets as illustrated in Fig. 4b.

The growth mechanism for ZnO single crystal flakes is believed to be similar to the one found for SnO$_2$ nanotube

arrays synthesized using the same combustion CVD process.[22] A simple direct vapor–solid (VS) conversion model can be applied to explain the growth of ZnO single crystal flakes. Initially, zinc nitrate precursor is decomposed and converted into ZnO vapor within the combustion flame. The resulting vapor species is then condensed on the relatively cold Si substrate, accumulating to a bulk layer. This stage continues for a relatively long period of time since there was no preferential growth of ZnO flakes observed under microscope even after 20 min of deposition. As condensation continues, the grains with energetically or kinetically favorable crystallographic planes will grow faster than the others. Once initiated, this preferential growth process will be accelerated since the top layer receives more ZnO vapor and also experiences higher temperature than the layer below. SEM images shown in Fig. 5 reveal different growth stages of ZnO flakes. Under these favorable growing conditions, ZnO single crystal flakes expand in two dimensions and gradually grow into cactus-like shape with wider top and narrower bottom. Although at a much smaller rate, ZnO vapor received at the root also contributes to the increase of the height. The same mechanism has been proposed to explain the growth of ZnO nanonails, which have large caps and very slim shafts.[23] Close observation reveals that each ZnO flake consists of layered structures with each layer in the thickness of 50 to 250 nm (Fig. 2e, Fig. 5a, 5b). During deposition, some layers could grow much faster than others. The final ZnO flake can be very thin (Fig. 2e, 2f). It is interesting to note in Fig. 2f, isolated small hexagonal ZnO layers could nucleate and grow on the surface of a larger flake. Nucleation on $\{0001\}$ polar surfaces

Fig. 6 A solid-state gas sensor based a single crystal ZnO flake. (a) SEM micrograph of the sensor consisting of a ZnO flake and Pt interdigitated electrodes, and (b) current variation with time under a constant voltage of 100 mV as sample gas was switched from air to different concentrations of ethanol vapor at 400 °C. Data were collected at one second intervals.
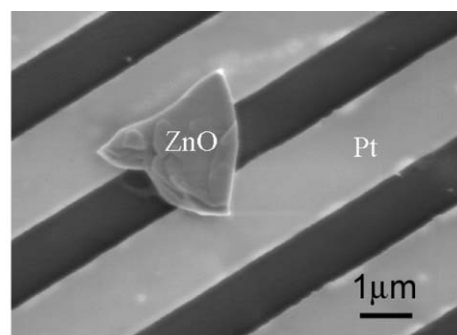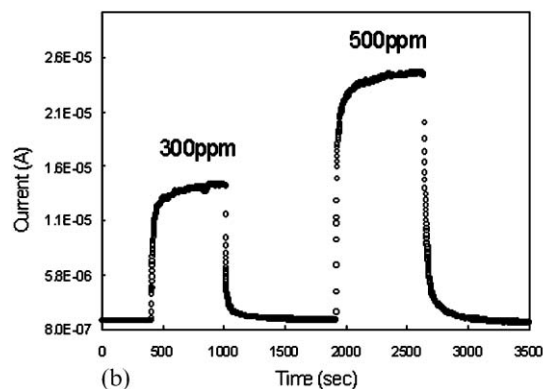

Fig. 5 SEM images of ZnO flakes taken at different stages of growth. Synthesis temperature was 1100 °C.

could be initiated by introducing planar defects to the polar surfaces.[24]

The width/thickness ratio of each ZnO single crystal flake ranged from 25 to 100. The large specific area of ZnO flakes would dramatically enhance the kinetics of electrochemical and catalytic processes. As a demonstration, a gas sensor was fabricated by placing a fraction of a ZnO flake onto interdigitated Pt electrodes, as shown in Fig. 6a. The thickness of the ZnO flake is about 200 nm. The sensor was tested at 400 °C in ethanol vapor. The performance of the ZnO flake sensor is shown in Fig. 6b; the sensor responded quickly as the gas was switched from air to different concentration of ethanol vapor and recovered fully when the gas was switched back to air.
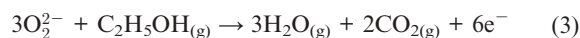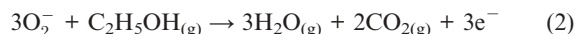
The response and recovery time is defined as the time needed to reach 90% of the full response ($R_f - R_0$), where R_f is the full-scale conductance when the sensor is in equilibrium with the ethanol vapor and R_0 is the baseline conductance when the sensor is in equilibrium with air. As shown in Fig. 6b, it took 62 s at 400 °C for the sensor to respond to ethanol vapor (reach 90% of its full response) and approximately the same amount of time to recover. The ratio of ($R_f - R_0$)/R_0 was 7.8 and 14.3 when the atmosphere was switched from air to 300 and 500 ppm ethanol vapor, respectively.

The gas sensing behavior of a semiconducting oxide can be attributed to both surface and bulk interactions, depending on grain size or film thickness. If grain size or film thickness is much larger than the Debye length λ_D of the material, the bulk interactions will dominate the sensor response. On the other hand, if grain size or film thickness is smaller than or in the same order of magnitude as λ_D, surface interactions will dominate the sensor behavior.[25,26] The large surface to volume ratio and small size of the ZnO flake sample suggest that ethanol–ZnO interactions on the surface may play an important role.

The interactions between ethanol and lattice oxygen O_O^X in a metal oxide such as ZnO can be described in general by the following defect reaction (in Kröger–Vink notation):

$$6O_O^X + C_2H_5OH_{(g)} \rightarrow 2CO_{2(g)} + 3H_2O_{(g)} + 6V_O^{\cdot\cdot} + 12e^- \quad (1)$$
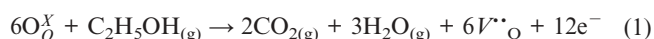
Similarly, the interactions between ethanol and the surface-adsorbed oxygen species[27] such as superoxide ion O_2^- and peroxide ion O_2^{2-} can be described as

$$3O_2^- + C_2H_5OH_{(g)} \rightarrow 3H_2O_{(g)} + 2CO_{2(g)} + 3e^- \qquad (2)$$

$$3O_2^{2-} + C_2H_5OH_{(g)} \rightarrow 3H_2O_{(g)} + 2CO_{2(g)} + 6e^- \qquad (3)$$

These reactions produce more electrons and thus increase the conductivity of ZnO (n-type) upon exposure to ethanol. The dependence of conductivity on partial pressure of ethanol can be derived from these reactions using mass–action law and charge neutrality relations. It is noted, however, that these reactions are very general and schematic; ethanol molecules may dissociate to other intermediate species before oxidation at ZnO surfaces. However, identification of the intermediates requires some sensitive surface spectroscopic techniques and tremendous effort. Investigation into the detailed sensing mechanisms is still underway and will be reported subsequently.

Conclusions

Using a combustion CVD process, we have successfully synthesized a new two-dimensional structure, ZnO single crystal flakes. The flakes grew upward from the underneath Si substrate. The as-grown ZnO flakes were typically 200 nm thick and 10–20 μm wide. Unlike most 1-D ZnO structures with [0001] growth direction, ZnO flakes grow along $<10\bar{1}0>$ directions. Gas sensor based on a 200 nm thick ZnO flake exhibited high sensitivity and fast response to ethanol vapor.

Acknowledgements

Ying Liu,[a] **Jian Dong,**[a] **Peter J. Hesketh**[b] **and Meilin Liu**[*a]
[a]Center for Innovative Fuel Cell and Battery Technologies, School of Materials Science and Engineering, Georgia Institute of Technology, Atlanta, GA, 30332-0245, USA. E-mail: meilin.liu@mse.gatech.edu; Fax: 1 404 894 9140; Tel: 1 404 894 6114
[b]School of Mechanical Engineering, Georgia Institute of Technology, Atlanta, GA, 30332-0405, USA

References

1 T. Seiyama and A. Kato, *Anal. Chem.*, 1962, **34**, 1502.
2 H. W. Ryu, B. S. Park, S. A. Akbar, W. S. Lee, K. J. Hong, Y. J. Seo, D. C. Shin, J. S. Park and G. P. Choi, *Sens. Actuators, B.*, 2003, **96**, 717.
3 D. F. Paraguay, M. Miki-Yoshida, J. Morales, J. Solis and L. W. Estrada, *Thin Solid Films*, 2000, **373**, 137.
4 D. Gruber, F. Kraus and J. Müller, *Sens. Actuators, B.*, 2003, **92**, 81.
5 W. J. Moon, J. H. Yu and G. M. Choi, *Sens. Actuators, B.*, 2002, **87**, 464.
6 H. M. Lin, S. J. Tzeng, P. J. Hsiau and W. L. Tsai, *Nanostruct. Mater.*, 1998, **10**, 465.
7 X. L. Cheng, H. Zhao, L. H. Huo, S. Gao and J. G. Zhao, *Sens. Actuators, B.*, 2004, **102**, 248.
8 C. Baratto, G. Sberveglieri, A. Onischuk, B. Caruso and S. di Stasio, *Sens. Actuators, B.*, 2004, **100**, 261.
9 H. Kind, H. Q. Yan, B. Messer, M. Law and P. D. Yang, *Adv. Mater.*, 2002, **14**, 158.
10 P. D. Yang, H. Q. Yan, S. Mao, R. Russo, J. Johnson, R. Saykally, N. Morris, J. Pham, R. R. He and H. J. Choi, *Adv. Funct. Mater.*, 2002, **12**, 323.
11 S. C. Lyu, Y. Zhang, C. J. Lee, H. Ruh and H. J. Lee, *Chem. Mater.*, 2003, **15**, 3294.
12 Y. K. Tseng, C. J. Huang, H. M. Cheng, I. N. Lin, K. S. Liu and I. C. Chen, *Adv. Funct. Mater.*, 2003, **13**, 811.
13 Z. L. Wang, *Mater. Today*, 2004, **6**, 26.
14 Y. Liu, S. Zha and M. Liu, *Adv. Mater.*, 2004, **16**, 256.
15 Y. Liu, W. Rauch, S. Zha and M. Liu, *Solid State Ionics*, 2004, **166**, 261.
16 A. T. Hunt, W. B. Carter and J. K. Cochran, *Appl. Phys. Lett.*, 1993, **63**, 266.
17 Y. Liu, C. Compson and M. Liu, *J. Power Sources*, 2004, **138**, 194.
18 J. Q. Hu, Q. Li, N. B. Wong, C. S. Lee and S. T. Lee, *Chem. Mater.*, 2002, **14**, 1216.
19 J. J. Wu and S. C. Liu, *Adv. Mater.*, 2002, **14**, 215.
20 P. X. Gao, Y. Ding and Z. L. Wang, *Nano Lett.*, 2003, **3**, 1315.
21 Z. W. Pan, Z. R. Dai and Z. L. Wang, *Science*, 2001, **291**, 1947.
22 Y. Liu, J. Dong and M. Liu, *Adv. Mater.*, 2004, **16**, 353.
23 J. Y. Lao, J. Y. Huang, D. Z. Wang and Z. F. Ren, *Nano Lett.*, 2003, **3**, 235.
24 Z. L. Wang, *J. Phys.: Condens. Matter*, 2004, **16**, R829.
25 M. Radecka, K. Zakrzewska and M. Rekas, *Sens. Actuators, B.*, 1998, **47**, 194.
26 N. Barsan and U. Weimar, *J. Electroceram.*, 2001, **7**, 143.
27 D. Kohl, *Sens. Actuators, B.*, 1989, **18**, 71.